Since January 2020 Elsevier has created a COVID-19 resource centre with free information in English and Mandarin on the novel coronavirus COVID-19. The COVID-19 resource centre is hosted on Elsevier Connect, the company's public news and information website.

3

Normalizing images is good to improve computer-assisted COVID-19 diagnosis

Claudio Filipi Gonçalves dos Santos[1], Leandro Aparecido Passos[2], Marcos Cleison de Santana[2], João Paulo Papa[2]

[1]*DEPARTMENT OF COMPUTING, FEDERAL UNIVERSITY OF SÃO CARLOS, SÃO CARLOS, BRAZIL;* [2]*DEPARTMENT OF COMPUTING, SÃO PAULO STATE UNIVERSITY, BAURU, BRAZIL*

1. Introduction

Coronavirus Disease 2019 (COVID-19) is supposed to have emerged in a local seafood market in Wuhan City, China, in December 2019, resembling an unknown cause viral pneumonia [1]. Further analysis from the lower respiratory tract pointed out the origin of the problem: a novel virus from Coronaviridae family, whence named SARS-CoV-2, supposedly originated from Phinolophus bats [2]. Four months later, the virus has spread from Wuhan to the whole world, producing a global public health crisis with no precedented, and reporting a total of 123,010 deaths and 1,914,916 confirmed infections as of 10:00 CET, April 15, 2020 [3]. Moreover, contingency methods adopted to withhold the outbreak, most of them based on quarantine and social isolation, are also assembling a global economic recession, whose results are unpredictable at the moment.

In such an apocalyptic scenario, the scientific community has been working frantically toward the development of vaccines, drugs, and biological resources to ease the contamination and the spread of the disease. On the other hand, computational and mathematical tools are being developed to improve the preciseness while predicting the contamination evolution, as well as defining new methods for detecting the disease. Regarding the latter, the diagnosis confirmation is performed through reverse transcription of a polymerase chain reaction (RT-PCR), or gene sequencing for respiratory or blood specimens [4]. However, such processes present some drawbacks related to a limitation of samples and available material to perform the analysis. The aforementioned limitations become exceptionally intolerable, once patients not identified in time and appropriately treated constitute a risk for themselves, as well as for the population in general since they can infect a large number of people given the highly contagious nature of the virus.

Data Science for COVID-19. https://doi.org/10.1016/B978-0-12-824536-1.00033-2

A possible alternative for a fast diagnosis may reside over chest X-ray [4,5]. It was observed that almost all patients with COVID-19 present intrinsic radiographic features depicting abnormalities in the bilateral involvement [1], including multifocal patchy consolidation, ground-glass opacities, and interstitial changes with a peripheral distribution [6]. Such patterns, however, are only moderately characteristic for the human eye [7], therefore requiring intelligent computer-aided assistance for boosting the diagnosis for both speed and reliability.

Machine learning–based algorithms have been successfully employed to tackle virtually any topic related to medicine in the last decades, ranging from Parkinson's disease [8] to breast [9,10] and esophagus [11] cancer detection. Moreover, with the advent of deep models, i.e., artificial neural networks composed of subsequent layers of simpler models capable of extracting more intrinsic information from the data [12], the number of works has grown exponentially, most of the times obtaining as good as or even better results than the ones performed by humans, with an extra advantage of demanding a small fraction of the time.

In this context, Wang et al. [13] proposed the COVID-Net, an open-source deep convolutional neural network (CNN) designed to detect COVID-19 cases from chest radiography, obtaining relevant results over the COVID Chest X-ray Dataset [14]. Despite their success, the model proposed by the authors still present limited results, even more considering a relatively high number of parameters to be learned, which implies directly in the time required for training. Therefore, this work proposes employing an EfficientNet-B6 [15] inspired neural network empowered with a data normalization approach to the task of COVID-19 detection on chest X-ray images, resulting in a lighter and faster CNN, capable of dealing with data scarcity and a highly imbalanced dataset.

Thus, the contributions of this work are twofold: (i) to propose the use of an EfficientNet-B6-based CNN empowered with a pixel normalization approach to deal with chest X-ray images in the context of COVID-19 and (ii) to support the scientific community in the combat of the most astonishing pandemic endured in the modern times. The remainder of this work is presented as follows. Section 2 provides a brief theoretical background concerning coronavirus disease 2019, while Section 3 describes the proposed approach. Furthermore, Sections 4 and 5 state the methodology and the experimental results, respectively. Finally, Section 6 asserts the conclusions and future work.

2. Coronavirus disease 2019

SARS-CoV-2, the coronavirus causing COVID-19, provides similar damage as the plasmodium, responsible for malaria, once both desaturates the body by removing iron from the heme molecule, thus inhibiting the flow of oxygen through the body, which is performed by the hemoglobin. The process is carried out while the lungs are still entirely operating, so there is no necessity of intubation or similar precautions. However, the problems concerning the respiratory process occur because the iron is then deposited in the lungs, which provides the frosted glass stains in X-ray exams. Once the lungs are

impregnated with iron, the patient starts the severe acute respiratory syndrome (SARS). In theory, COVID-19 is a hematological disease, targeting the cells of the blood, causing the pulmonary problems a severe secondary effect of the oxidative iron released in the lungs [16].

In general, the clinical manifestations resemble viral pneumonia, whose approximately 80% of cases are mild and present self-limiting symptoms that demand 2 weeks for recovery [17]. Considering the remaining 20% cases, patients present severe conditions with acute respiratory distress syndrome and septic shock, eventually ended in multiple organ failure [18].

Regarding the pathology, histological lung examinations revealed proteinaceous exudate, edema, and focal hyperplasia of pneumocytes with only inconsistent inflammatory cellular infiltration on COVID-19 early-stage patients [18]. Patients in a later stage are prone to present bilateral diffuse alveolar damage with exudative lesions in the lung, interstitial inflammatory cells, multinucleated syncytial cells with atypical enlarged pneumocytes, as well as a substantial decrease on CD4+ and CD8+ T cells, which implies on severe immune injuries [19].

Finally, considering COVID-19 treatment, there is no specific antiviral therapies or vaccine to date. Therefore, researches toward the development of new drugs, as well as randomized controlled tests over existing ones, are of paramount importance at the moment. In this context, medical interventions are divided into four [18] groups: (i) general treatment, (ii), coronavirus-specific treatments, (iii) antiviral treatments, and (iv) other.

The general treatment includes nutritional interventions to boost the immune system and Chinese medicine, such as Chloroquine, successfully employed to treat malaria. Experiments considering the latter presented good results over COVID-19 in vitro [20], as well as patients by promoting a virus negative conversion, shortening the disease course, and reducing exacerbation of pneumonia [21]. Coronavirus-specific treatments focus on vaccines and therapies related to the S-protein [22], successfully employed in the treatment of virus SARS-CoV and MERS-CoV [23]. Concerning antiviral treatments, no candidate solution provided satisfactory results for COVID-19 to date [24]. On the other hand, the "remdesivir," an antiviral being developed to treat Ebola virus infection [25], has revealed itself as effective and secure to treat COVID-19 [20]. Finally, concerning other methods, Le et al. [26] employed the IL-6 inhibitor Tocilizumab to combat the surplus of cytokine produced by the immune system. At the same time, Chen et al. [27] recommend influenza and Streptococcus pneumoniae vaccination, thus avoiding confusion concerning similar symptoms or even a combination infection of both COVID-19 and one of them.

3. Proposed approach

EfficientNets are a family of CNN architecture designed over a baseline network, which is scaled to obtain several models with distinct characteristics [15]. Among such models,

Table 3.1 EfficientNet-B6 composition. Notice that Conv, BN, and Activation denote the operations of convolution, batch normalization, and the activation using the Swish [31] function, respectively. Besides, MBConvBlock stands for the network's main blocks.

Level	Operation	Kernel size	Channels	Repetitions
0	Conv, BN, activation	3	56	1
1	MBConvBlock	3	56	3
2	MBConvBlock	3	240	6
3	MBConvBlock	5	432	6
4	MBConvBlock	3	864	8
5	MBConvBlock	5	1200	8
6	MBConvBlock	5	2064	11
7	MBConvBlock	3	3456	3
8	Conv, BN, activation	1	2304	1

EfficientNet-B6 obtained notorious influence in the scientific community due to its efficiency and accuracy while dealing with image classification, confirming its robustness over several different data sets [28–30]. A schema of the network blocks is detailed in Table 3.1.

The core of the network resides on a stack of layers built upon a structure called MBConvBlock. Each of these structures is composed of a set of operations. The DWConv, for instance, acts as a depth-wise convolution operation. The BatchNorm and Activation block execute the batch normalization and the Swish [31] activation function, respectively. Furthermore, the Squeeze block performs a global average pooling, while the Reduce block performs a convolution over a reduced number of kernels (usually $1/4$), followed by a Swish activation. Furthermore, the Expand block denotes a convolution layer with sigmoid activation, while the Excite layer stands for an element-wise multiplication between the Activation and Expand blocks. Moreover, the Projection and the Dropout blocks perform a convolution with a kernel size of one and a dropout procedure, respectively. Finally, the Add block executes the addition between the original input and the Dropout block output. Fig. 3.1 depicts the structure.

Finally, two approaches were considered to improve the model efficiency.[1] The first comprises the computational burden and stands for a change in the architecture input size from 528×528 to 224×224. Such a change provided competitive results with about a third of the baseline model [13] parameters. The second regards a data normalization in the range $[-1, 1]$, which provided considerable improvements in the classification results.

[1]Available at https://github.com/cfsantos/EffNet-B6-COVID19.

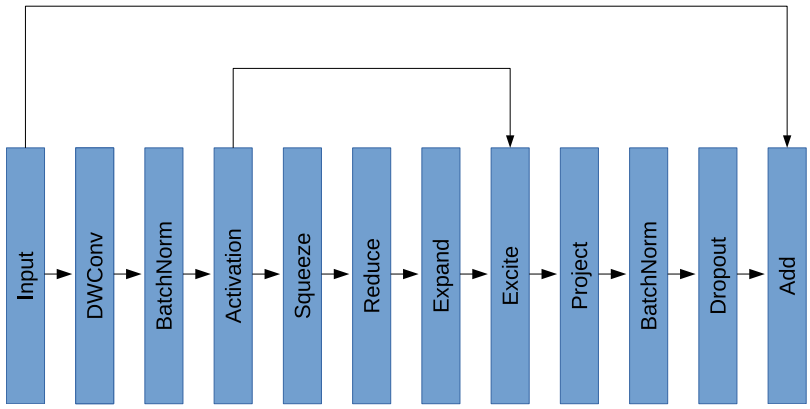

FIGURE 3.1 The MBConvBlock structure, in which the arrows stand for the skip connections.

4. Methodology

This section provides a detailed description of the dataset and the experimental setup employed in this work.

4.1 Datasets

The experiments performed in this chapter were conducted over a combination of chest X-ray images from two public datasets: the COVID-19 image data collection [14] and the Kaggle RSNA Pneumonia Detection Challenge.[2] The combination comprises four classes of images, i.e., Bacterial Pneumonia (Bacterial), Viral Pneumonia (Viral), and COVID-19 patients (COVID-19), as well as healthy people (Health). Fig. 3.2 provides a sample example from each class.

Finally, the combination of datasets comprises a total of 6,042 chest X-ray image samples, being 1,583 from class "Health," 2,792 from "Bacterial Pneumonia," 1,515 from "Viral Pneumonia," and 152 images from "COVID-19" patients. Besides, the dataset was split into 5,394 randomly selected samples for training and 648 samples for testing purposes. Such a splitting methodology is the same employed by Ref. [13], whose results are considered as a baseline for comparison purposes.

4.2 Experimental setup

The experiments conducted in this work rely on a model pretrained during 50 epochs over the training set, with no transfer learning. Furthermore, the weights that accomplish the best results, i.e., the state of the network at the epoch the model performed best, are reloaded. Then the model is trained for more 50 epochs using artificial data

[2]Available at https://www.kaggle.com/c/rsna-pneumonia-detection-challenge/.

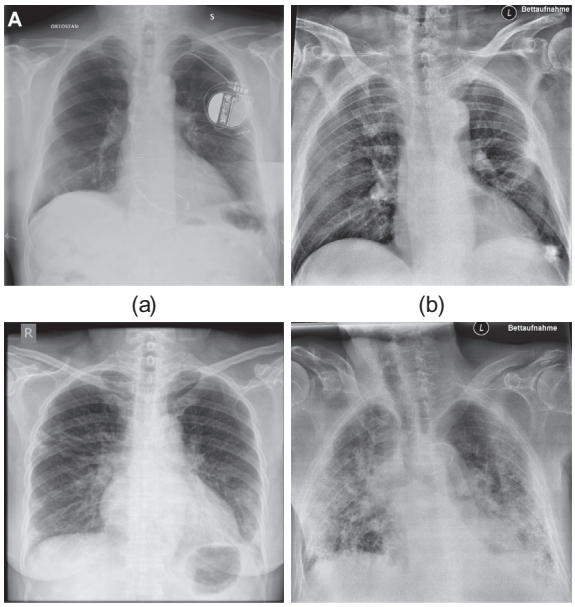

FIGURE 3.2 Examples of images X-ray images from: (A) health [32], (B) bacterial [33], (C) viral [34], and (D) COVID-19 [33][3].

augmentation, provided by the Keras Image Augmentation API [35], which performs transformations such as random rotation, shifts, shear, and flips over the original training dataset.

For comparison purposes, the work considers the COVID-Net [13], a tailored-made deep neural network to detect X-rays with or without COVID-19, as the baseline. Besides, the performance of the model is also compared against the standard version of the EfficientNet-B6 with naive data normalization. Finally, the model employs the RMSProp [36] algorithm as the optimization algorithm and a batch of size 4. Furthermore, the data augmentation procedure considers a rotation range between 0 and 30°, width and height random shift of 20%, random zoom between 0 and 15%, and a random horizontal flip. The model is developed using Keras [35] and TensorFlow [37].

5. Experimental results

This section presents the experimental results considering the EfficientNet-B6 based approach for COVID-19 detection on chest X-ray images. Furthermore, it also provides a brief discussion about such results and model's performance.

[3]Under licence: (a) and (c) https://creativecommons.org/licenses/by-nc-nd/4.0/, and (b) and (d) https://creativecommons.org/licenses/by/3.0/.

5.1 Results

Table 3.2 presents an overall comparison between the proposed approach and the COVID-Net. The baseline approach outperformed the proposed method in 5% considering the accuracy value; however, at the cost of almost three times the number of parameters to be learned. Concerning the computational burden, the method proposed in this work required around 17 h to perform the complete training step, as well as less than 0.02 s for inference considering an NVIDIA Tesla P4 with 8 Gb of RAM machine.[4] The COVID-Net authors did not provide the elapsed time for training and inference, but the number of multiply-accumulation operations instead.

Table 3.3 presents the results of the proposed method against two baselines: the COVID-Net and the standard version of the EfficientNet. Results are compared considering three distinct metrics: (i) the sensitivity, also known as recall, (ii) the positive predictive value (PPV), also known as precision, and (iii) f1-score, which is the average of precision and recall over in each class, i.e., health, bacterial pneumonia, virus pneumonia, and COVID-19. The best results are in bold.

Fig. 3.3 depicts the confusion matrix concerning the proposed approach.

Table 3.2 Comparison between the proposed model and COVID-Net features.

Model	Params(M)	MAC	Training (H)	Inference (s)	Accuracy(%)
EfficientNet-B6	40.9	–	17.1	0.0018	86.5
COVID-Net	116.6	2.26	–	–	83.5

Table 3.3 Results concerning the Sensitivity, PPV, and F1-Score (in %) for each class and model. Notice Normalized EfficientNet-B6 stand for the proposed approach.

		Class			
Metric(%)	Method	Health	Bacterian	Viral	COVID19
Sensitivity	COVID-Net	73.9	93.1	**81.9**	**100.0**
	Standard EfficientNet-B6	81.6	**94.3**	79.3	94.4
	Normalized EfficientNet-B6	**84.1**	93.9	78.6	94.4
PPV	COVID-Net	**95.1**	87.1	67.0	80.0
	Standard EfficientNet-B6	93.6	**88.5**	77.2	60.7
	Normalized EfficientNet-B6	92.9	86.8	**78.6**	**85.0**
F1-score	COVID-NET	84.5	90.1	74.4	**90.0**
	Standard EfficientNet-B6	87.2	**91.3**	78.2	73.9
	Normalized EfficientNet-B6	**88.3**	90.2	**78.6**	89.4

[4]Notice the experiments may have been conducted on a computer with different settings.

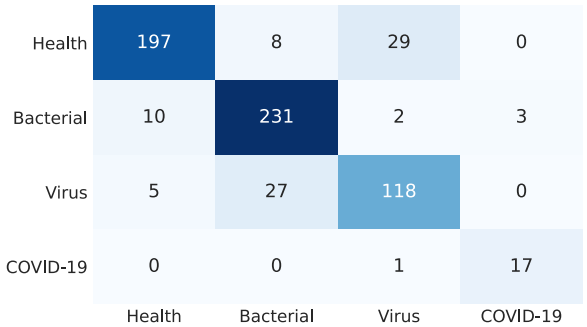

FIGURE 3.3 Normalized EfficientNet-B6 confusion matrix. The X-axis represents the predicted value, while the Y-axis stands for the true labels.

5.2 Discussion

According to the results, COVID-Net and EfficientNet performed very similarly at some points. Nevertheless, it is valid to discuss each class according to its numbers.

- "Health" class performed very well for detecting positive instances for all the three neural networks, reaching values over 90%. The proposed approach obtained the best Sensitivity and F1-score values, which figures the more complicated scenarios due to the elevated number of "Viral" wrongly predicted as "Health," as shown in Fig. 3.3.
- 'Bacterial" images obtained the highest values considering all metrics, in general, and performed well overall three techniques, being the Standard EfficientNet-B6 the most accurate. COVID-Net performed somewhat more competent for discarding negative cases while Normalized EfficientNet-B6 performed slightly better for predicting positive instances.
- "Viral" pneumonia presented the worst results considering the three networks in general. Concerning the Standard EfficientNet-B6, approximately 25% of its validation images were predicted as "Health." Notwithstanding, the Normalized EfficientNet-B6 performed better than COVID-Net and standard EfficientNet-B6 considering the PPV and F1 metrics.
- "COVID-19" presented an appropriate classification rate over the three networks. In this context, the proposed method was the most effective while predicting positive values, obtaining a PPV rate of 85%. The major drawback in this context concerns the number of available instances for validation purposes, being eight images deemed for COVID-Net and 18 for EfficientNet-B6.

The Normalized EfficientNet-B6 performs better than the standard version of the network in the overall result, except for "Bacterian" class. In addition, it also provided competitive results when compared to COVID-Net, with the advantage of a considerably reduced number of parameters. It shows the normalization values between -1 and 1, in this specific case, arranges the data in a geometric space that facilitates and improves the training of the neural network.

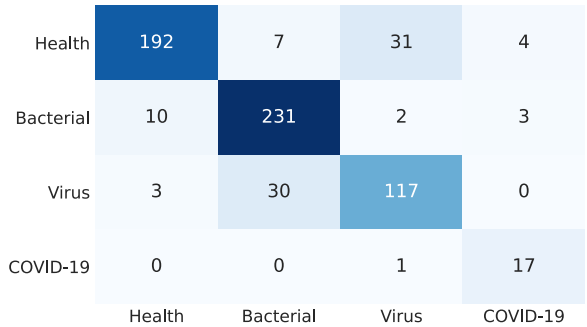

FIGURE 3.4 Confusion matrix of the model using test-time augmentation. X-axis shows the predicted value while the Y-axis shows the true labels.

An additional test-time augmentation experiment was conducted to analyze COVID-19 sensitiveness regarding pneumonia cases. In this context, for each testing sample, 50 artificial instances were created by using random width and height shifts of 5%, and then the model performed the prediction. Furthermore, the final result of a given instance is provided by the votation over 50 predictions. Fig. 3.4 presents the confusion matrix considering such a scenario. Notice the overall result remains similar to the original, despite the sensitivity regarding "COVID-19" class. In such a case, some "Health" images were erroneously predicted as "COVID-19," thus dropping the PPV in almost 15%. The reason for such behavior probably lies in the lack of "COVID-19" images available for training purposes.

The lack of available images expresses an even worse situation when considering medical issues due to the patient's privacy, the unavailability of specialists to evaluate the data, as well as other problems. Such an absence is especially problematic for deep learning models since they demand an extensive amount of data for a proper generalization over real-world scenarios. Moreover, the dataset provides another challenging drawback related to data imbalance, since it comprises, for instance, $1,515$ bacterial pneumonia X-ray images, while, on the other hand, it bears only 152 images characterizing COVID-19 exams.

6. Conclusions and future works

This study demonstrates the possibility of improving results toward COVID-19 chest X-ray image detection through deep learning-based approaches by normalizing the input images' pixel values between $[-1, 1]$ instead of the traditional $[0, 1]$ approach. Such conditions allow smaller neural networks to perform better than bigger and more complex networks, under some circumstances.

Although the EfficientNet family of networks is among the most powerful known classifiers, such models still present an open room for some improvements toward more trustful classifiers for evaluating the health conditions of patients in real-world problems. On the other hand, a more considerable amount of data available for training is

also capable of providing secure predictions in the context. One can assume, from now on, that the number of samples concerning COVID-19 patients tends to grow proportionally to the number of infected people, thus providing more accurate results.

Regarding future work, our goal is to continually search for methods to improve the EfficientNet family of models, as well as several other machine learning–based approaches for COVID-19 or other disease detection. Furthermore, we also intend to perform similar experiments considering a more significative number of COVID-19 samples and distinct architectures for the tasks of feature extraction and classification.

Acknowledgments

The authors acknowledge FAPESP grants #2013/07375-0, #2014/12236-1, #2017/25908-6, and #2019/07665-4, and CNPq grants 307066/2017-7 and 427968/2018-6.

References

[1] C. Huang, Y. Wang, X. Li, L. Ren, J. Zhao, Y. Hu, L. Zhang, G. Fan, J. Xu, X. Gu, et al., Clinical features of patients infected with 2019 novel coronavirus in wuhan, China, Lancet 395 (10223) (2020) 497–506.

[2] W.H. Organization, et al., Clinical Management of Severe Acute Respiratory Infection when Novel Coronavirus (2019-ncov) Infection Is Suspected: Interim Guidance, World Health Organization, 2020, 28 January 2020. Tech. Rep.

[3] W.H. Organization, et al., Coronavirus Disease 2019 (Covid-19): Situation Report, 2020, p. 85.

[4] T. Ai, Z. Yang, H. Hou, C. Zhan, C. Chen, W. Lv, Q. Tao, Z. Sun, L. Xia, Correlation of chest ct and rt-pcr testing in coronavirus disease 2019 (covid-19) in China: a report of 1014 cases, Radiology (2020) 200642.

[5] Y. Fang, H. Zhang, J. Xie, M. Lin, L. Ying, P. Pang, W. Ji, Sensitivity of chest Ct for Covid-19: comparison to Rt-Pcr, Radiology (2020) 200432.

[6] M. Chung, A. Bernheim, X. Mei, N. Zhang, M. Huang, X. Zeng, J. Cui, W. Xu, Y. Yang, Z.A. Fayad, et al., Ct imaging features of 2019 novel coronavirus (2019-ncov), Radiology 295 (1) (2020) 202–207.

[7] M.Y. Ng, E.Y. Lee, J. Yang, F. Yang, X. Li, H. Wang, M.M.s. Lui, C.S.Y. Lo, B. Leung, P.L. Khong, et al., Imaging profile of the covid-19 infection: radiologic findings and literature review, Radiology 2 (1) (2020) e200,034.

[8] L.A. Passos, C.R. Pereira, E.R. Rezende, T.J. Carvalho, S.A. Weber, C. Hook, J.P. Papa, Parkinson disease identification using residual networks and optimum-path forest, in: 2018 IEEE 12th International Symposium on Applied Computational Intelligence and Informatics (SACI), IEEE, 2018, pp. 000,325–000,330.

[9] L.A. Passos, C. Santos, C.R. Pereira, L.C.S. Afonso, J.P. Papa, A hybrid approach for breast mass categorization, in: ECCOMAS Thematic Conference on Computational Vision and Medical Image Processing, Springer, 2019, pp. 159–168.

[10] P.B. Ribeiro, L.A. Passos, L.A. da Silva, K.A. da Costa, J.P. Papa, R.A. Romero, Unsupervised breast masses classification through optimum-path forest, in: 2015 IEEE 28th International Symposium on Computer-Based Medical Systems, IEEE, 2015, pp. 238–243.

[11] L.A. Passos, L.A. de Souza Jr., R. Mendel, A. Ebigbo, A. Probst, H. Messmann, C. Palm, J.P. Papa, Barrett's esophagus analysis using infinity restricted Boltzmann machines, J. Vis. Commun. Image R. 59 (2019) 475–485.

[12] Y. LeCun, Y. Bengio, G.E. Hinton, Deep learning, Nature 521 (7553) (2015) 436–444.

[13] L. Wang, A. Wong, Covid-net: A Tailored Deep Convolutional Neural Network Design for Detection of Covid-19 Cases from Chest Radiography Images, 2020 arXiv preprint arXiv:2003.09871.

[14] J.P. Cohen, P. Morrison, L. Dao, Covid-19 Image Data Collection, 2020 arXiv preprint arXiv:2003.11597.

[15] M. Tan, Q.V. Le, Efficientnet: Rethinking Model Scaling for Convolutional Neural Networks, 2019 arXiv preprint arXiv:1905.11946.

[16] W. Liu, H. Li, Covid-19: Attacks the 1-beta Chain of Hemoglobin and Captures the Porphyrin to Inhibit Human Heme Metabolism.

[17] Z. Wu, J.M. McGoogan, Characteristics of and important lessons from the coronavirus disease 2019 (covid-19) outbreak in China: summary of a report of 72 314 cases from the Chinese center for disease control and prevention, Jama 323 (13) (2020) 1239–1242. https://doi.org/10.1001/jama.2020.2648.

[18] M. Xie, Q. Chen, Insight into 2019 novel coronavirus an updated intrim review and lessons from sars-cov and mers-cov, Int. J. Infect. Dis. 94 (2020) 119–124. https://doi.org/10.1016/j.ijid.2020.03.071.

[19] Z. Xu, L. Shi, Y. Wang, J. Zhang, L. Huang, C. Zhang, S. Liu, P. Zhao, H. Liu, L. Zhu, et al., Pathological findings of covid-19 associated with acute respiratory distress syndrome, Lancet Res. Med. 8 (4) (2020) 420–422.

[20] M. Wang, R. Cao, L. Zhang, X. Yang, J. Liu, M. Xu, Z. Shi, Z. Hu, W. Zhong, G. Xiao, Remdesivir and chloroquine effectively inhibit the recently emerged novel coronavirus (2019-ncov) in vitro, Cell Res, 30 (3) (2020) 269–271.

[21] J. Gao, Z. Tian, X. Yang, Breakthrough: chloroquine phosphate has shown apparent efficacy in treatment of covid-19 associated pneumonia in clinical studies, Biosci. Trends 14 (1) (2020) 72–73. https://doi.org/10.5582/bst.2020.01047.

[22] M. Hoffmann, H. Kleine-Weber, S. Schroeder, N. Krüger, T. Herrler, S. Erichsen, T.S. Schiergens, G. Herrler, N.H. Wu, A. Nitsche, et al., Sars-cov-2 cell entry depends on ace2 and tmprss2 and is blocked by a clinically proven protease inhibitor, Cell 181 (2) (2020) 271–280. https://doi.org/10.1016/j.cell.2020.02.052.

[23] J. Sui, W. Li, A. Murakami, A. Tamin, L.J. Matthews, S.K. Wong, M.J. Moore, A.S.C. Tallarico, M. Olurinde, H. Choe, et al., Potent neutralization of severe acute respiratory syndrome (sars) coronavirus by a human mab to s1 protein that blocks receptor association, Proc. Natl. Acad. Sci. U.S.A. 101 (8) (2004) 2536–2541.

[24] J. Chen, Y. Ling, X. Xi, P. Liu, F. Li, T. Li, Z. Shang, M. Wang, Y. Shen, H. Lu, Efficacies of lopinavir/ritonavir and abidol in the treatment of novel coronavirus pneumonia, Chin. J. Infect. Dis. 38 (0) (2020) E008.

[25] S. Mulangu, L.E. Dodd, R.T. Davey Jr., O. Tshiani Mbaya, M. Proschan, D. Mukadi, M. Lusakibanza Manzo, D. Nzolo, A. Tshomba Oloma, A. Ibanda, et al., A randomized, controlled trial of ebola virus disease therapeutics, N. Engl. J. Med. 381 (24) (2019) 2293–2303.

[26] R.Q. Le, L. Li, W. Yuan, S.S. Shord, L. Nie, B.A. Habtemariam, D. Przepiorka, A.T. Farrell, R. Pazdur, Fda approval summary: tocilizumab for treatment of chimeric antigen receptor t cell-induced severe or life-threatening cytokine release syndrome, Oncology 23 (8) (2018) 943.

[27] Q. Chen, L. Wang, M. Xie, X. Li, Recommendations for influenza and streptococcus pneumoniae vaccination in elderly people in China, Aging Med. 3 (1) (2020) 1–11. https://doi.org/10.1002/agm2.12102.

[28] A. Krizhevsky, G. Hinton, et al., Learning Multiple Layers of Features from Tiny Images, 2009.

[29] T. Berg, J. Liu, S. Woo Lee, M.L. Alexander, D.W. Jacobs, P.N. Belhumeur, Birdsnap: large-scale fine-grained visual categorization of birds, in: Proceedings of the IEEE Conference on Computer Vision and Pattern Recognition, 2014, pp. 2011−2018.

[30] S. Maji, E. Rahtu, J. Kannala, M. Blaschko, A. Vedaldi, Fine-grained Visual Classification of Aircraft, 2013 arXiv preprint arXiv:1306.5151.

[31] P. Ramachandran, B. Zoph, Q.V. Le, Searching for Activation Functions, CoRR abs/1710.05941, 2017. URL, http://arxiv.org/abs/1710.05941.

[32] E. Ebrille, M.T. Lucciola, C. Amellone, F. Ballocca, F. Orlando, M. Giammaria, Syncope as the presenting symptom of covid-19 infection, HeartRhythm Case Rep. (2020).

[33] H.B. Winther, H. Laser, S. Gerbel, S.K. Maschke, J.B. Hinrichs, J. Vogel-Claussen, F.K. Wacker, M.M. HÃper, B.C. Meyer, Covid-19 Image Repository, 2020. https://doi.org/10.6084/m9.figshare.12275009.v1. URL, https://figshare.com/articles/dataset/COVID-19_Image_Repository/12275009/1.

[34] A. Hamimi, Mers-cov: Middle east respiratory syndrome corona virus: can radiology be of help? initial single center experience, Egyp. J. Radiol. Nucl. Med. 47 (1) (2016) 95−106.

[35] F. Chollet, et al., Keras, 2015.

[36] Y.N. Dauphin, H. de Vries, J. Chung, Y. Bengio, Rmsprop and Equilibrated Adaptive Learning Rates for Non-convex Optimization, 2015. CoRR abs/1502.04390, URL, http://arxiv.org/abs/1502.04390.

[37] M. Abadi, A. Agarwal, P. Barham, E. Brevdo, Z. Chen, C. Citro, G.S. Corrado, A. Davis, J. Dean, M. Devin, S. Ghemawat, I. Goodfellow, A. Harp, G. Irving, M. Isard, Y. Jia, R. Jozefowicz, L. Kaiser, M. Kudlur, J. Levenberg, D. Mané, R. Monga, S. Moore, D. Murray, C. Olah, M. Schuster, J. Shlens, B. Steiner, I. Sutskever, K. Talwar, P. Tucker, V. Vanhoucke, V. Vasudevan, F. Viégas, O. Vinyals, P. Warden, M. Wattenberg, M. Wicke, Y. Yu, X. Zheng, TensorFlow: Large-Scale Machine Learning on Heterogeneous Systems, 2015. URL, www.tensorflow.org/ (Software available from: tensorflow.org).